

# The dynamics of starvation and recovery

2 Justin D. Yeakel \* †‡, Christopher P. Kempes †, and Sidney Redner †§

3 \*School of Natural Science, University of California Merced, Merced, CA, †The Santa Fe Institute, Santa Fe, NM, §Department of Physics, Boston University, Boston  
4 MA, and ‡To whom correspondence should be addressed: jdyeakel@gmail.com

5 Submitted to Proceedings of the National Academy of Sciences of the United States of America

6 The eco-evolutionary dynamics of species is fundamentally linked  
7 to the energetic constraints of its constituent individuals. Of par-  
8 ticular importance are the tradeoffs between reproduction and  
9 the dynamics of starvation and recovery in resource-limited envi-  
10 ronments. To elucidate the consequences of this tradeoff, we  
11 introduce a minimal nutritional state-structured model that in-  
12 corporates two classes of consumer: nutritionally replete con-  
13 sumers that reproduce, and undernourished, non-reproducing  
14 consumers that are susceptible to mortality. As a function of the  
15 transition rates between these replete and undernourished states  
16 that are determined by the presence or absence of resources,  
17 the consumer populations can either undergo cyclic dynamics or  
18 reach a steady state. We obtain strong constraints on starvation  
19 and recovery rates by deriving allometric scaling relationships  
20 and find that population dynamics subject to these constraints  
21 can approach the cyclic regime but are typically driven to a steady  
22 state. Moreover, we find that these rates fall within a ‘refuge’ in pa-  
23 rameter space, where the probability of extinction of the consumer  
24 population is minimized. Thus we identify a potential mechanism  
25 that may both drive and constrain the dynamics of animal pop-  
26ulations. Our model provides a natural framework that predicts  
27 maximum body size for mammals by determining the relative sta-  
28 bility of an otherwise homogeneous population to a mutant pop-  
29 ulation with altered percent body fat. For body masses  $\lesssim 10^7$  g,  
30 individuals with increased energetic reserves can invade resident  
31 populations, and vice versa for body mass  $\gtrsim 10^7$  g, thus providing  
32 a principled mechanism for a within-lineage driver of Cope’s rule.

33 foraging | starvation | reproduction

## 34 Introduction

35 The behavioral ecology of all organisms is influenced by the en-  
36 ergetic state of individuals, which directly influences how they  
37 invest reserves in uncertain environments. Such behaviors are  
38 generally manifested as tradeoffs between investing in somatic  
39 maintenance and growth, or allocating energy towards repro-  
40 duction [1, 2, 3]. The timing of these behaviors responds to  
41 selective pressure, as the choice of the investment impacts fu-  
42 ture fitness [4, 5, 6]. The influence of resource limitation on an  
43 organism’s ability to maintain its nutritional stores may lead to  
44 repeated delays or shifts in reproduction over the course of an  
45 organism’s life.

46 The balance between (a) somatic growth and maintenance,  
47 and (b) reproduction is often conditioned on resource availabil-  
48 ity [7]. For example, reindeer invest less in calves born after  
49 harsh winters (when the mother’s energetic state is depleted)  
50 than in calves born after moderate winters [8]. Many bird  
51 species invest differently in broods during periods of resource  
52 scarcity compared to normal periods [9, 10], sometimes delaying  
53 or even foregoing reproduction for a breeding season [1, 11, 12].  
54 Even freshwater and marine zooplankton have been observed to  
55 avoid reproduction under nutritional stress [13], and those that  
56 do reproduce have lower survival rates [2]. Organisms may also  
57 separate maintenance and growth from reproduction over space  
58 and time: many salmonids, birds, and some mammals return to  
59 migratory breeding grounds to reproduce after one or multiple  
60 seasons in resource-rich environments where they accumulate  
61 nutritional reserves [14, 15, 16].

62 Physiology also plays an important role in regulating re-  
63 productive expenditures during periods of resource limitation.  
64 The data collected thus far has shown that diverse mammals (47

65 species in 10 families) exhibit delayed implantation, whereby fe-  
66 males postpone fetal development (blastocyst implantation) un-  
67 til nutritional reserves can be accumulated [17, 18]. Many other  
68 many species (including humans) suffer irregular menstrual cy-  
69 cling and higher spontaneous abortion rates during periods of  
70 nutritional stress [19, 20]. In the extreme case of unicellular  
71 organisms, nutrition is unavoidably linked to reproduction be-  
72 cause the nutritional state of the cell regulates all aspects of the  
73 cell cycle [21]. The existence of so many independently evolved  
74 mechanisms across such a diverse suite of organisms highlights  
75 the importance and universality of the fundamental tradeoff  
76 between somatic and reproductive investment. However the  
77 dynamic implications of these constraints are unknown.

78 Though straightforward conceptually, incorporating the en-  
79 ergetic dynamics of individuals [22] into a population-level  
80 framework [22, 23] presents numerous mathematical obsta-  
81 cles [24]. An alternative approach involves modeling the  
82 macroscale relations that guide somatic versus reproductive  
83 investment in a consumer-resource system. For example,  
84 macroscale Lotka-Volterra models assume that the growth rate  
85 of the consumer population depends on resource density, thus  
86 implicitly incorporating the requirement of resource availability  
87 for reproduction [25].

88 In this work, we adopt an alternative approach in which we  
89 explicitly account for resource limitation and the subsequent  
90 effect of starvation. Namely, only individuals with sufficient en-  
91 ergetic reserves can reproduce. Such a constraint leads to repro-  
92 ductive time lags due to some members of the population going  
93 hungry and then recovering. Additionally, we incorporate the  
94 idea that reproduction is strongly constrained allometrically[3],  
95 and is not generally linearly related to resource density. As we  
96 shall show, these constraints influence the ensuing population  
97 dynamics in dramatic ways.

98 **99 Nutritional state-structured model (NSM)**  
100 We begin by defining a minimal Nutritional State-structured  
101 population Model (NSM), where the consumer population is  
102 partitioned into two states: (a) an energetically replete (full)  
103 state  $F$ , where the consumer reproduces at a constant rate  $\lambda$   
104 and does not die from starvation, and (b) an energetically de-  
105 ficient (hungry) state  $H$ , where the consumer does not repro-  
106 duce but dies by starvation at rate  $\mu$ . The underlying resource  
107  $R$  evolves by logistic growth with an intrinsic growth rate  $\alpha$   
108 and a carrying capacity equal to one. Consumers transition  
109 from the full state  $F$  to the hungry state  $H$  at a rate  $\sigma$ —the

---

## Reserved for Publication Footnotes

starvation rate—and also in proportion to the absence of re-  
 sources ( $1 - R$ ). Conversely, consumers recover from state  $H$  to state  $F$  at rate  $\rho$  and in proportion to  $R$ . Resources are also eaten by the consumers—at rate  $\rho$  by hungry consumers and at rate  $\beta < \rho$  by full consumers. This inequality accounts for hungry consumers requiring more resources to replace lost body tissue. The NSM represents a fundamental extension of the idealized starving random walk model of foraging, which focuses on resource depletion, to include reproduction and source replenishment [?, ?, ?].

In the mean-field approximation, in which the consumers and resources are perfectly mixed, their densities evolve according to the rate equations

$$\begin{aligned}\dot{F} &= \lambda F + \rho RH - \sigma(1 - R)F, \\ \dot{H} &= \sigma(1 - R)F - \rho RH - \mu H, \\ \dot{R} &= \alpha R(1 - R) - R(\rho H + \beta F).\end{aligned}$$

Notice that the total consumer density  $F + H$  evolves according to  $\dot{F} + \dot{H} = \lambda F - \mu H$ . This resembles the equation of motion for the predator density in the classic Lotka-Volterra model [?], except that the resource density does not appear in the growth term. As discussed above, the attributes of reproduction and mortality have been explicitly apportioned to the full and hungry consumers, respectively, so that the growth in the total density is decoupled from the resource density.

Equation [1] has three fixed points: two trivial fixed points at  $(F^*, H^*, R^*) = (0, 0, 0)$  and  $(0, 0, 1)$ , and one non-trivial, internal fixed point at

$$\begin{aligned}F^* &= \frac{\alpha\lambda\mu(\mu + \rho)}{(\lambda\rho + \mu\sigma)(\lambda\rho + \mu\beta)}, \\ H^* &= \frac{\alpha\lambda^2(\mu + \rho)}{(\lambda\rho + \mu\sigma)(\lambda\rho + \mu\beta)}, \\ R^* &= \frac{\mu(\sigma - \lambda)}{\lambda\rho + \mu\sigma}.\end{aligned}$$

The stability of this fixed point is determined by the Jacobian matrix  $\mathbf{J}$ , where each matrix element  $J_{ij} = \partial\dot{X}_i/\partial X_j$  when evaluated at the internal fixed point, and  $\mathbf{X}$  is the vector  $(F, H, R)$ . The parameters in Eq. [1] are such that the real part of the largest eigenvalue of  $\mathbf{J}$  is negative, so that the system is stable with respect to small perturbations from the fixed point. Because this fixed point is unique, it is the global attractor for all population trajectories for any initial condition where the resource and consumer densities are both nonzero.

From Eq. [2], an obvious constraint on the NSM is that the reproduction rate  $\lambda$  must be less than the starvation rate  $\sigma$ , so that  $R^*$  is positive. In fact, when the resource density  $R = 0$ , the rate equation for  $F$  gives exponential growth of  $F$  for  $\lambda > \sigma$ . The condition  $\sigma = \lambda$  represents a transcritical (TC) bifurcation [?] that demarcates the physical regime from the physical regime where  $F$  would grow exponentially with time. The biological implication of the constraint  $\lambda < \sigma$  has a simple interpretation—the rate at which a macroscopic organism loses mass due to lack of resources is generally much faster than the rate of reproduction. As we will discuss below, this inequality is a natural consequence of allometric constraints [3] for organisms within empirically observed body size ranges (Fig. 2).

In the physical regime of  $\lambda < \sigma$ , the fixed point [2] may either be a stable node or a limit cycle (Fig. 3). In continuous-time systems, a limit cycle arises when a pair of complex conjugate eigenvalues crosses the imaginary axis to attain positive real parts [26]. This Hopf bifurcation is defined by  $\text{Det}(\mathbf{S}) = 0$ , with  $\mathbf{S}$  the Sylvester matrix, which is composed of the coefficients of the characteristic polynomial of the Jacobian ma-

stable regime but close to the Hopf bifurcation, the amplitude of the transient but decaying cycles become large. Given that logical systems are constantly being perturbed [28], the onset of transient cycles, even though they decay with time in the mean-field description, can increase the extinction risk [29, 30, 31]. Thus the distance of a system from the Hopf bifurcation vides a measure of its persistence.

When the starvation rate  $\sigma \gg \lambda$ , a substantial fraction of the consumers are driven to the hungry non-reproducing state. Because reproduction is inhibited, there is a low steady-state consumer density and a high steady-state resource density. However, if  $\sigma/\lambda \rightarrow 1$  from above, the population is overloaded with energetically-replete (reproducing) individuals, thereby promoting oscillations between the consumer and resource densities (Fig. 3).

Whereas the relation between consumer growth rate  $\lambda$  and the starvation rate  $\sigma$  defines an absolute bound of biological feasibility—the TC bifurcation— $\sigma$  also determines the sensitivity of the consumer population to changes in resource density. When  $\sigma \gg \lambda$ , the steady-state population density is small, thereby increasing the risk of stochastic extinction. On the other hand, as  $\sigma$  decreases, the system will ultimately be poised either near the TC or the Hopf bifurcation (Fig. 3). If the recovery rate  $\rho$  is sufficiently small, the TC bifurcation is reached and the resource eventually is eliminated. If  $\rho$  exceeds a threshold value, cyclic dynamics will develop as the Hopf bifurcation is approached.

### Role of allometry

While there are no a priori constraints on the parameters in the NSM, most organisms correspond to restricted portions of the parameter space. Here we use allometric scaling relations to constrain the covariation of rates in a principled and biologically meaningful manner. Allometric scaling relations highlight common constraints and average trends across large ranges in body size and species diversity. Many of these relations can be derived from a small set of assumptions and below we describe a

framework to determine the covariation of timescales and rates across the range of mammals for each of the key parameters of our model (cf. [32]). We are thereby able to define the regime of dynamics occupied by the entire class of mammals along with the key differences between the largest and smallest mammals.

Nearly all of the rates described in the NSM are determined by consumer metabolism, which can be used to describe a variety of organismal features [33]. The scaling relation between an organism's metabolic rate  $B$  and its body mass  $M$  at reproductive maturity is known to scale as  $B = B_0 M^\eta$  [34], where the scaling exponent  $\eta$  is typically close to 2/3 or 3/4 for metazoans (e.g., [33]), and has taxonomic shifts for unicellular species between  $\eta \approx 1$  in eukaryotes and  $\eta \approx 1.76$  in bacteria [35, 3]. An organism's metabolic rate  $B$  is proportional to the cost of tissue maintenance in the absence of growth (i.e., when the body mass is  $M$ ). By definition  $B = \beta/\xi$ , where  $\beta$  is the rate at which resources are consumed for full consumers (see Eq. [1]) and where  $\xi$  is related to the conversion efficiency of resource to consumer tissue (Supporting Information, section XX).

Several efforts have shown how a partitioning of  $B$  between growth and maintenance purposes can be used to derive a general equation for both the growth trajectories and growth rates of organisms ranging from bacteria to metazoans [36, 37, 38, 39, 3]. This relation is derived from the simple balance condition [36, 37, 38, 39, 3]

$$B_0 m^\eta = E_m \dot{m} + B_m m, \quad [3]$$

222  $m$  is the mass of the organism at any point in its development. 222 of an organism, the above energy balance prescribes the mass  
223 This balance has the general solution [40, 3] 223 trajectory of a non-consuming organism:

$$\left(\frac{m(t)}{M}\right)^{1-\eta} = 1 - \left[1 - \left(\frac{m_0}{M}\right)^{1-\eta}\right] e^{-a(1-\eta)t/M^{1-\eta}} \quad [4]$$

$$m(t) = M e^{-a't/M^{1-\eta}}. \quad [9]$$

224 where, for  $\eta < 1$ ,  $M = (B_0/B_m)^{1/(1-\eta)}$  is the asymptotic mass,  
225  $a = B_0/E_m$ , and  $m_0$  is mass at birth. We now use this solution  
226 to define the timescale (see [37] for a detailed presentation of  
227 these timescales) of reproduction and recovery from starvation.  
228 The time that it takes to reach a particular mass  $\epsilon M$  is given  
229 by the timescale

$$\tau(\epsilon) = \ln \left[ \frac{1 - (m_0/M)^{1-\eta}}{1 - \epsilon^{1-\eta}} \right] \frac{M^{1-\eta}}{a(1-\eta)} \quad [5]$$

230 where we will define values of  $\epsilon$  to describe a set of rates within  
231 our model. For the time to reproduce,  $t_\lambda = \tau(\epsilon_\lambda)$ , where  $\epsilon_\lambda$  is  
232 the fraction of the asymptotic mass where an organism is repro-  
233 ductively mature and should be close to one (typically  $\epsilon_\lambda \approx 0.95$   
234 [36]). The growth rate is then given by  $\lambda = \ln(v)/t_\lambda$  where  $v$  is  
235 the number of offspring produced, and for any constant value of  
236  $\epsilon_\lambda$  this will scale like  $\lambda \propto M^{\eta-1}$  for  $M \gg m_0$  [36, 37, 38, 39, 3].

237 The rate of recovery  $\rho = 1/t_\rho$  requires that an organism  
238 accrues sufficient tissue to transition from the hungry to the  
239 full state. Since only certain tissues can be digested for energy  
240 (for example the brain cannot be degraded to fuel metabolism),  
241 we define the rates for starvation, death, and recovery by the  
242 timescales required to reach, or return from, specific fractions of  
243 the replete-state mass (see the Supporting Information for de-  
244 tails on these parameterizations). We define  $m_\sigma = \epsilon_\sigma M$ , where  
245  $\epsilon_\sigma < 1$  is the fraction of replete-state mass where reproduc-  
246 tion ceases. This fraction will be modified if tissue composition  
247 systematically scales with adult mass. For example, making  
248 use of the observation that body fat in mammals scales with  
249 overall body size according to  $M_{\text{fat}} = f_0 M^\gamma$  and assuming that  
250 once this mass is fully digested the organism starves, this would  
251 imply that  $\epsilon_\sigma = 1 - f_0 M^\gamma / M$ . It follows that the recovery  
252 timescale,  $t_\rho$ , is the time to go from  $m = \epsilon_\sigma \epsilon_\lambda M$  to  $m = \epsilon_\sigma M$   
253 (Figure 1). Using Eqs. [4] and [5] this timescale is given by  
254 simply considering an adjusted starting mass of  $m'_0 = \epsilon_\sigma \epsilon_\lambda M$ ,  
255 in which case

$$t_\rho = \ln \left[ \frac{1 - (\epsilon_\sigma \epsilon_\lambda)^{1-\eta}}{1 - \epsilon^{1-\eta}} \right] \frac{M^{1-\eta}}{a'(1-\eta)} \quad [6]$$

256 where  $a' = B_0/E'_m$  accounts for possible deviations in the  
257 biosynthetic energetics during recovery (see Supporting Infor-  
258 mation). It should be noted that more complicated ontogenetic  
259 models explicitly handle storage [39], whereas this feature is  
260 implicitly covered by the body fat scaling in our framework.

261 To determine the starvation rate,  $\sigma$ , we are interested in the  
262 time required for an organism to go from a mature adult that  
263 reproduces at rate  $\lambda$ , to a reduced-mass hungry state where re-  
264 production is impossible. For starving individuals we assume  
265 that an organism must meet its maintenance requirements using  
266 the digestion of existing mass as the sole energy source. This  
267 assumption implies the following simple metabolic balance

$$\dot{m}E'_m = -B_m m$$

268 or

$$\dot{m} = -\frac{a'}{M^{1-\eta}} m$$

269 where  $E'_m$  is the amount of energy stored in a unit of exist-  
270 ing body mass which differs from  $E_m$ , the energy required to  
271 synthesize a unit of biomass [39]. Given the replete mass,  $M$ ,

272 of an organism, the above energy balance prescribes the mass  
273 trajectory of a non-consuming organism:

$$t_\sigma = -\frac{M^{1-\eta}}{a'} \ln(\epsilon_\sigma). \quad [10]$$

274 The time scale for starvation is given by the time it takes  $m(t)$   
275 to reach  $\epsilon_\sigma M$ , which gives

$$276 \quad \text{The starvation rate is then } \sigma = 1/t_\sigma, \text{ which scales with replete-} \\ 277 \quad \text{state mass as } 1/M^{1-\eta} \ln(1 - f_0 M^\gamma / M). \text{ An important feature} \\ 278 \quad \text{is that } \sigma \text{ does not have a simple scaling dependence on } \lambda, \text{ which} \\ 279 \quad \text{is important for the dynamics that we later discuss.}$$

280 The time to death should follow a similar relation, but de-  
281 fined by a lower fraction of replete-state mass,  $m_\mu = \epsilon_\mu M$ .  
282 Suppose, for example, that an organism dies once it has di-  
283 gested all fat and muscle tissues, and that muscle tissue scales  
284 with body mass according to  $M_{\text{musc}} = u_0 M^\zeta$ . This gives  
285  $\epsilon_\mu = 1 - (f_0 M^\gamma + u_0 M^\zeta) / M$ . Muscle mass has been shown  
286 to be roughly proportional to body mass [41] in mammals and  
287 thus  $\epsilon_\mu$  is merely  $\epsilon_\sigma$  minus a constant. The time to death is the  
288 total time to reach  $\epsilon_\mu M$  minus the time to starve, or

$$t_\mu = -\frac{M^{1-\eta}}{a'} \ln(\epsilon_\mu) - t_\sigma, \quad [11]$$

289 and  $\mu = 1/t_\mu$ .

290 Although the rate equations [1] are general, here we focus  
291 on parameterizations for terrestrial-bound endotherms, specif-  
292 ically mammals, which range from a minimum of  $M \approx 1$   
293 gram (the Etruscan shrew *Suncus etruscus*) to a maximum of  
294  $M \approx 10^7$  grams (the late Eocene to early Miocene Indricotheri-  
295 inae). Investigating other classes of organisms would simply  
296 involve altering the metabolic exponents and scalings associate  
297 with  $\epsilon$ . Moreover, we emphasize that our allometric equations  
298 describe mean relationships, and do not account for the (some-  
299 times considerable) variance associated with individual species.

### 300 Stabilizing effects of allometric constraints

301 As the allometric derivations of the NSM rate laws reveal, star-  
302 vation and recovery rates are not independent parameters, and  
303 the biologically relevant portion of the phase space shown in  
304 Fig. 3 is constrained via covarying parameters. Given the pa-  
305 rameters of terrestrial endotherms, we find that  $\sigma$  and  $\rho$  are  
306 constrained to lie within a small window of potential values  
307 (Fig. 4) for the known range of body sizes  $M$ . We thus find  
308 that the dynamics for all mammalian body sizes is confined to  
309 the steady-state regime of the NSM and that limit-cycle behav-  
310 ior is precluded. Moreover, for larger  $M$ , the distance to the  
311 Hopf bifurcation increases, while uncertainty in allometric pa-  
312 rameters (20% variation around the mean; Fig. 4) results in  
313 little qualitative difference in the distance to the Hopf bi-  
314 furcation. These results suggest that small mammals are more  
315 prone to population oscillations—both stable limit cycles and  
316 transient cycles—than mammals with larger body size. Thus  
317 our NSM model predicts that population cycles should be less  
318 common for larger species and more common for smaller species,  
319 particularly in environments where resources are limiting.

320 It should be noted that previous studies have used allomet-  
321 ric constraints to explain the periodicity of cyclic populations  
322 [42, 43, 44], suggesting a period  $\propto M^{0.25}$ . However this relation  
323 seems to hold only for some species [45], and potential drivers  
324 range from predator and/or prey lifespans to competitive dy-  
325 namics [46, 47]. Statistically significant support for the exis-  
326 tence of population cycles among mammals is predominantly  
327 based on time series for small mammals [48], where our model

hand, the longer gestational times and the increased difficulty in measurements, precludes obtaining similar-quality data for larger organisms.

### Extinction risk

Within our model, higher rates of starvation result in a larger flux of the population to the hungry state. In this state reproduction is absent, thus increasing the likelihood of extinction. From the perspective of population survival, it is the rate of starvation relative to the rate of recovery that determines the long-term dynamics of the various species (Fig. 3). We therefore examine the competing effects of cyclic dynamics vs. changes in steady state density on extinction risk as a function of the ratio  $\sigma/\rho$ . To this end, we computed the probability of extinction, where we define extinction as a population trajectory falling below one fifth of the allometrically constrained steady state at any time between  $10^6$  and  $\leq 10^8$ . This procedure is repeated for 1000 replicates of the continuous-time system shown in Eq. 1 for an organism of  $M = 100$  grams. In each replicate the initial densities are chosen to be  $A(F^*, H^*, R^*)$ , with  $A$  a random variable that is uniformly distributed in [0, 2]. By allowing the rate of starvation to vary, we assessed extinction risk across a range of values of  $\sigma/\rho$  between ca.  $10^{-3}$  to 5, thus examining a horizontal cross-section of Fig. 3. As expected, higher rates of extinction correlate with both low and high values of  $\sigma/\rho$ . For low values of  $\sigma/\rho$ , the increased extinction risk results from transient cycles with larger amplitudes as the system nears the Hopf bifurcation (Fig. 5). For large values of  $\sigma/\rho$ , higher extinction risk arises because of the decrease in the steady state consumer population density. This interplay creates an ‘extinction refuge’ as shown in Fig. 5, such that for a constrained range of  $\sigma/\rho$ , extinction probabilities are minimized.

We find that the allometrically constrained values of  $\sigma/\rho$  (with 20% variability around energetic parameter means) fall within the extinction refuge. These values are close enough to the Hopf bifurcation to avoid low steady state densities, and far enough away to avoid large-amplitude transient cycles. The fact that allometric values of  $\sigma$  and  $\rho$  fall within this relatively small window supports the possibility that a selective mechanism has constrained the physiological conditions that drive starvation and recovery rates within populations. Such a mechanism would select for organism physiology that generates appropriate  $\sigma$  and  $\rho$  values that avoid extinction. This selection could occur via the tuning of body fat percentages, metabolic rates, and biomass maintenance efficiencies. To summarize, our finding that the allometrically-determined parameters fall within this low extinction probability region suggests that the NSM dynamics may both drive—and constrain—natural animal populations.

Dynamic and energetic barriers to body size

Metabolite transport constraints are widely thought to place strict boundaries on biological scaling [49, 50, 33] and thereby lead to specific predictions on the minimum possible body size for organisms [51]. Above this bound, a number of energetic and evolutionary mechanisms have been explored to assess the costs and benefits associated with larger body masses, particularly for mammals. One important such example is the *fasting endurance hypothesis*, which contends that larger body size, with consequent lower metabolic rates and increased ability to maintain more endogenous energetic reserves, may buffer organisms against environmental fluctuations in resource availability [52]. Over evolutionary time, terrestrial mammalian lineages show a significant trend towards larger body size (known as Cope’s Rule) [53, 54, 55, 56], and it is thought that within-lineage

drivers generate selection towards an optimal upper bound of roughly  $10^7$  grams [53], whose value may arise from higher extinction risk for large taxa over evolutionary timescales [54]. These trends are thought to be driven by a combination of climate change and niche availability [56]; however the underlying pinning energetic costs and benefits of larger body sizes, and how they influence dynamics over ecological timescales, have not been explored. We argue that the NSM provides a suitable framework to explore these issues.

The NSM correctly predicts that species with smaller masses have larger steady-state population densities (Fig. 6a). It should also be noted that  $R^*$  is decreasing for increasing body size. From the perspective of classic resource competition theory we would expect that the species that can live on the lowest resource abundance should outcompete others [57, 58, 59]. The NSM then predicts that larger mammals should outcompete smaller ones, supporting the ‘copes rule’. This is a natural consequence of the steady-state dynamics combined with the derived timescales.

Furthermore, many previous studies have focused on the energy equivalence hypothesis which argues that the total energy use,  $B_{tot}$ , of a population is constant independent of species size (e.g. [60, 61]). This hypothesis is based on observations showing that the abundance,  $N$ , of a species is proportional to the inverse of individual metabolism (e.g.  $N \propto M^{-3/4}/B_0$ ) (e.g. [60, 61]). This is usually stated as  $B_{tot} = NB = \text{constant}$  which has been shown to hold in mammalian and vascular plant communities (e.g. [60, 61]). Figure ?? shows that both  $F^*$  and  $H^*$  scale like  $M^{-\eta}$  over a wide range of organism sizes and Figure ?? shows that  $F^*B$  is a constant over this same range. This result is remarkable because it illustrates that the steady state values of the NSM combined with the derived timescales naturally give rise to the energy equivalence result. Furthermore, the equivalence breaks down at distinct sizes at both the large and small end of mammals suggesting that these are hard limits on mammalian body sizes because organisms outside this range do not meet the constant efficiency obeyed by other populations. Significant deviations from constant energy use occur at  $M \lesssim 1$  at the small end of mammals and  $M \approx 6.5 * 10^7$  for the large end. Compellingly, this dynamic bound, which is determined by the rate of energetic recovery, is close to the minimum observed mammalian body size of ca. 1.3–2.5 grams (Fig. 6b,c), a range that occurs as the recovery rate begins its decline. In addition to known transport limitations [51], we suggest that an additional constraint of lower body size stems from the dynamics of starvation. This result mirrors other efforts [3, 62] where at a given scale multiple limitations constrain the smallest possibilities for life within a class of organisms.

A additional theoretical upper bound on mammalian body size is given by  $\epsilon = 0$ , where mammals are entirely composed of metabolic reserves, and this occurs at a size of  $M = 8.3 \times 10^8$ , or  $4.5 \times$  the mass of a blue whale. We determine a more realistic upper bound to body mass by assessing the susceptibility of an otherwise homogeneous population to invasion by a mutated subset of the population (denoted by  $'$ ) where individuals have a modified proportion of body fat  $M' = M(1 + \chi)$  where  $\chi \in [-0.5, 0.5]$ , thus altering the rates of starvation  $\sigma$ , recovery  $\rho$ , and maintenance  $\beta$ . There is no internal fixed point that correspond to a state where both original residents and invaders coexist (except for the trivial state  $\chi = 0$ ). To assess the susceptibility to invasion as a function of the invader mass, we determine which consumer has a higher steady-state density for a given value of  $\chi$ . We find that for  $1 \leq M < 10^6$  g, having additional body fat ( $\chi > 0$ ) results in a higher steady-state invader population density ( $H'^* + F'^* > H^* + F^*$ ). Thus the invader has an intrinsic advantage over the resident popu-

462 lation. However, for  $M > 10^6$ , leaner individuals ( $\chi < 0$ ) have 485 findings, suggest that the modern diversity of mammals may  
463 advantageous steady state densities. 486 not represent a true steady state the current distribution of

464 The observed switch in susceptibility as a function of  $\chi$  at 487 nutrients and large seeds may be very different from the past  
465  $M_{\text{opt}} \approx 10^6$  thus serves as an attractor, or an uninvadible evo- 488 [63, 64, 65].

466 lutionary stable state, such that the NSM predicts organismal 489 The energetics associated with somatic maintenance,  
467 mass to increase if  $M < M_{\text{opt}}$  and decrease if  $M > M_{\text{opt}}$ . More- 490 growth, and reproduction are important elements that influence  
468 over,  $M_{\text{opt}}$ , which is entirely determined by the population-level 491 the dynamics of all populations [11]. The NSM is a minimal and  
469 consequences of energetic constraints, is within an order of mag- 492 general model that incorporates the dynamics of starvation that  
470 nitude of the mass observed in the North American mammalian 493 are expected to occur in resource-limited environments. By in-  
471 fossil record [53] and also the mass predicted from an evolution- 494 corporating allometric relations between the rates in the NSM,  
472 ary model of body size evolution [54]. While the state of the 495 we found: (i) different organismal masses have distinct popu-  
473 environment, as well as the competitive landscape, will deter- 496 lation dynamic regimes, (ii) allometrically-determined rates of  
474 mine whether specific body sizes are selected for or against [56], 497 starvation and recovery appear to minimize extinction risk, and  
475 we suggest that the starvation dynamics outlined here may pro- 498 (iii) the dynamic consequences of these rates may place addi-  
476 vide the driving mechanism for the evolution of larger body size 499 tional barriers on the evolution of minimum and maximum body  
477 among terrestrial mammals. 500 size. We suggest that the NSM offers a means by which the dy-

478 One might be concerned a greater number of large mam- 501 namic consequences of energetic constraints can be assessed us-  
479 mals are currently not observed in the modern world given that 502 ing macroscale interactions between and among species. Future  
480 larger mammals are less susceptible to extinction. However, 503 efforts will involve exploring the consequences of these dynamics  
481 recent research suggests that the pleistocene may have been 504 in a spatially explicit framework, thus incorporating elements  
482 much more populated with a significant diversity of very large 505 such as movement costs and spatial heterogeneity, which may  
483 mammals [63, 64, 65] which were also much more geographi- 506 elucidate additional tradeoffs associated with the dynamics of  
484 cally widespread than today. These results, combined with our 507 starvation.

- 508 1. Martin TE (1987) Food as a Limit on Breeding Birds: A Life-History Perspective. *Annu. Rev. Ecol. Syst.* 18:453–487.
- 509 2. Kirk KL (1997) Life-History Responses to Variable Environments: Starvation and 510 Reproduction in Planktonic Rotifers. *Ecology* 78:434–441.
- 511 3. Kempes CP, Dutkiewicz S, Follows MJ (2012) Growth, metabolic partitioning, and 512 the size of microorganisms. *PNAS* 109:495–500.
- 513 4. Mangel M, Clark CW (1988) *Dynamic Modeling in Behavioral Ecology* (Princeton 514 University Press, Princeton).
- 515 5. Mangel M (2014) Stochastic dynamic programming illuminates the link between 516 environment, physiology, and evolution. *B. Math. Biol.* 77:857–877.
- 517 6. Yeakel JD, Dominy NJ, Koch PL, Mangel M (2014) Functional morphology, stable 518 isotopes, and human evolution: a model of consilience. *Evolution* 68:190–203.
- 519 7. Morris DW (1987) Optimal Allocation of Parental Investment. *Oikos* 49:332.
- 520 8. Tveraa T, Fauchald P, Henaug C, Yoccoz NG (2003) An examination of a com- 521 pensatory relationship between food limitation and predation in semi-domestic 522 reindeer. *Oecologia* 137:370–376.
- 523 9. Daan S, Dijkstra C, Drent R, Meijer T (1988) *Food supply and the annual timing of 524 avian reproduction*.
- 525 10. Jacot A, Valcu M, van Oers K, Kempenaers B (2009) Experimental nest site lim- 526 itation affects reproductive strategies and parental investment in a hole-nesting 527 passerine. *Animal Behaviour* 77:1075–1083.
- 528 11. Stearns SC (1989) Trade-Offs in Life-History Evolution. *Funct. Ecol.* 3:259.
- 529 12. Barboza P, Jorde D (2002) Intermittent fasting during winter and spring affects body 530 composition and reproduction of a migratory duck. *J Comp Physiol B* 172:419–434.
- 531 13. Threlkeld ST (1976) Starvation and the size structure of zooplankton communities. 532 *Freshwater Biol.* 6:489–496.
- 533 14. Weber TP, Ens BJ, Houston AI (1998) Optimal avian migration: A dynamic model 534 of fuel stores and site use. *Evolutionary Ecology* 12:377–401.
- 535 15. Mduma SAR, Sinclair ARE, Hilborn R (1999) Food regulates the Serengeti wilde- 536 beest: a 40-year record. *J. Anim. Ecol.* 68:1101–1122.
- 537 16. Moore JW, Yeakel JD, Peard D, Lough J, Beere M (2014) Life-history diversity and its 538 importance to population stability and persistence of a migratory fish: steelhead 539 in two large North American watersheds. *J. Anim. Ecol.* 83:1035–1046.
- 540 17. Mead RA (1989) in *Carnivore Behavior, Ecology, and Evolution* (Springer US, 541 Boston, MA), pp 437–464.
- 542 18. Sandell M (1990) The Evolution of Seasonal Delayed Implantation. *The Quarterly 543 Review of Biology* 65:23–42.
- 544 19. Bulik CM, et al. (1999) Fertility and Reproduction in Women With Anorexia Nervosa. 545 *J. Clin. Psychiatry* 60:130–135.
- 546 20. Trites AW, Donnelly CP (2003) The decline of Steller sea lions *Eumetopias jubatus* 547 in Alaska: a review of the nutritional stress hypothesis. *Mammal Review* 33:3–28.
- 548 21. Glazier DS (2009) Metabolic level and size scaling of rates of respiration and growth 549 in unicellular organisms. *Funct. Ecol.* 23:963–968.
- 550 22. Kooijman SALM (2000) *Dynamic Energy and Mass Budgets in Biological Systems* 551 (Cambridge).
- 552 23. Sousa T, Domingos T, Poggiale JC, Kooijman SALM (2010) Dynamic energy budget 553 theory restores coherence in biology. *Philos. T. Roy. Soc. B* 365:3413–3428.
- 554 24. Diekmann O, Metz JAJ (2010) How to lift a model for individual behaviour to the 555 population level? *Philos. T. Roy. Soc. B* 365:3523–3530.
- 556 25. Murdoch WW, Briggs CJ, Nisbet RM (2003) *Consumer-resource Dynamics*, Mono- 557 graphs in population biology (Princeton University Press).
- 558 26. Guckenheimer J, Holmes P (1983) *Nonlinear oscillations, dynamical systems, and 559 bifurcations of vector fields* (Springer, New York).
- 560 27. Gross T, Feudel U (2004) Analytical search for bifurcation surfaces in parameter 561 space. *Physica D* 195:292–302.
- 562 28. Hastings A (2001) Transient dynamics and persistence of ecological systems. *Ecol. Lett.* 4:215–220.
- 563 29. Neubert M, Caswell H (1997) Alternatives to resilience for measuring the responses 564 of ecological systems to perturbations. *Ecology* 78:653–665.
- 565 30. Caswell H, Neubert MG (2005) Reactivity and transient dynamics of discrete-time 566 ecological systems. *Journal of Difference Equations and Applications* 11:295–310.
- 567 31. Neubert M, Caswell H (2009) Detecting reactivity. *Ecology*.
- 568 32. Yodzis P, Innes S (1992) Body Size and Consumer-Resource Dynamics. *Am. Nat.* 569 139:1151–1175.
- 570 33. Brown J, Gillooly J, Allen A, Savage V, West G (2004) Toward a metabolic theory of 571 ecology. *Ecology* 85:1771–1789.
- 571 34. West GB, Woodruff WH, Brown JH (2002) Allometric scaling of metabolic rate from 572 molecules and mitochondria to cells and mammals. *Proc. Natl. Acad. Sci. USA* 99 Suppl 1:2473–2478.
- 573 35. DeLong JP, Okie JG, Moses ME, Sibly RM, Brown JH (2010) Shifts in metabolic 574 scaling, production, and efficiency across major evolutionary transitions of life. 575 *PNAS* 107:12941–12945.
- 576 36. West GB, Brown JH, Enquist BJ (2001) A general model for ontogenetic growth. 577 *Nature* 413:628–631.
- 578 37. Moses ME, et al. (2008) Revisiting a Model of Ontogenetic Growth: Estimating Model 579 Parameters from Theory and Data. <http://dx.doi.org.proxy.lib.sfu.ca/10.1086/679735> 171:632–645.
- 580 38. Gillooly JF, Charnov EL, West GB, Savage VM, Brown JH (2002) Effects of size and 581 temperature on developmental time. *Nature* 417:70–73.
- 582 39. Hou C, et al. (2008) Energy Uptake and Allocation During Ontogeny. *Science* 583 322:736–739.
- 584 40. Bettencourt LMA, Lobo J, Helbing D, Kuhnert C, West GB (2007) Growth, innovation, 585 scaling, and the pace of life in cities. *Proc. Natl. Acad. Sci. USA* 104:7301–7306.
- 586 41. Folland JP, Mc Cauley TM, Williams AG (2008) Allometric scaling of strength mea- 587 surements to body size. *Eur J Appl Physiol* 102:739–745.
- 588 42. Calder III WA (1983) An allometric approach to population cycles of mammals. *J. Theor. Biol.* 100:275–282.
- 589 43. Peterson RO, PAGE RE, DODGE KM (1984) Wolves, Moose, and the Allometry of 590 Population Cycles. *Science* 224:1350–1352.
- 591 44. Kruskal G, Schaffer WM (1991) Population cycles in mammals and birds: Does 592 periodicity scale with body size? *J. Theor. Biol.* 148:469–493.
- 593 45. Hendriks AJ, Mulder C (2012) Delayed logistic and Rosenzweig-MacArthur models 594 with allometric parameter setting estimate population cycles at lower trophic levels 595 well. *Ecological Complexity* 9:43–54.
- 596 46. Kendall BE, et al. (1999) Why do populations cycle? A synthesis of statistical and 597 mechanistic modeling approaches. *Ecology* 80:1789–1805.
- 598 47. Höglstedt G, Seldahl T, Breistol A (2005) Period length in cyclic animal populations. 599 *Ecology* 86:373–378.
- 600 48. Kendall, Prendergast, Bjørnstad (1998) The macroecology of population dynamics: 601 taxonomic and biogeographic patterns in population cycles. *Ecol. Lett.* 1:160–164.
- 602 49. Brown J, Marquet P, Taper M (1993) Evolution of body size: consequences of an 603 energetic definition of fitness. *Am. Nat.* 142:573–584.
- 604 605 606 607 608 609

- 610 50. West GB, Brown JH, Enquist BJ (1997) A General Model for the Origin of Allometric 632 60. Allen AP, Brown JH, Gillooly JF (2002) Global Biodiversity, Biochemical Kinetics, 611 Scaling Laws in Biology. *Science* 276:122–126. 633  
 612 51. West GB, Woodruff WH, Brown JH (2002) Allometric scaling of metabolic rate from 634 61. Enquist BJ, Brown JH, West GB (1998) Allometric scaling of plant energetics and 613 molecules and mitochondria to cells and mammals. *Proc. Natl. Acad. Sci. USA* 635 population density : Abstract : Nature. *Nature* 395:163–165.  
 614 52. Millar J, Hickling G (1990) Fasting Endurance and the Evolution of Mammalian 636 62. Kempes CP, Wang L, Amend JP, Doyle J, Hoehler T (2016) Evolutionary tradeoffs 615 Body Size. *Funct. Ecol.* 4:5–12. 637 in cellular composition across diverse bacteria. *ISME J* 10:2145–2157.  
 616 53. Alroy J (1998) Cope's rule and the dynamics of body mass evolution in North 638 63. Doughty CE, Wolf A, Malhi Y (2013) The legacy of the Pleistocene megafauna 617 American fossil mammals. *Science* 280:731. 639 extinctions on nutrient availability in Amazonia. *Nature Geosci* 6:761–764.  
 618 54. Clauset A, Redner S (2009) Evolutionary Model of Species Body Mass Diversifica- 640 64. Doughty CE, et al. (2016) Megafauna extinction, tree species range reduction, and 619 tion. *Phys. Rev. Lett.* 102:038103. 641 carbon storage in Amazonian forests. *Ecography* 39:194–203.  
 620 55. Smith F, Boyer A, Brown J, Costa D (2010) The Evolution of Maximum Body Size of 642 65. Doughty CE, Faurby S, Svenning JC (2016) The impact of the megafauna extinctions 621 Terrestrial Mammals. *Science*. 643 on savanna woody cover in South America. *Ecography* 39:213–222.  
 622 56. Saarinen JJ, et al. (2014) Patterns of maximum body size evolution in Cenozoic 644  
 623 land mammals: eco-evolutionary processes and abiotic forcing. *Proc Biol Sci* 281:20132049–20132049.  
 624 57. Tilman D (1981) Tests of Resource Competition Theory Using Four Species of Lake 645  
 625 Michigan Algae. *Ecology* 62:802–815.  
 626 58. Dutkiewicz S, Follows MJ, Bragg JG (2009) Modeling the coupling of ocean ecology 646 some for helpful discussions and comments on the manuscript. J.D.Y. was sup-  
 627 and biogeochemistry. *Global Biogeochem. Cycles* 23:n/a–n/a. 647 ported by startup funds at the University of California, Merced, and an Omidyar  
 628 59. Barton AD, Dutkiewicz S, Flierl G, Bragg J, Follows MJ (2010) Patterns of Diversity 648 Postdoctoral Fellowship at the Santa Fe Institute. C.P.K. was supported by an  
 629 in Marine Phytoplankton. *Science* 327:1509–1511. 649 Omidyar Postdoctoral Fellowship at the Santa Fe Institute. S.R. was supported  
 630 650 by grants DMR-1608211 and 1623243 from the National Science Foundation,  
 631 and by the John Templeton Foundation, all at the Santa Fe Institute.

644 **ACKNOWLEDGMENTS.** We thank Luis Bettancourt, Eric Libby, and Seth New-  
 645 some for helpful discussions and comments on the manuscript. J.D.Y. was sup-  
 646 ported by startup funds at the University of California, Merced, and an Omidyar  
 647 Postdoctoral Fellowship at the Santa Fe Institute. C.P.K. was supported by an  
 648 Omidyar Postdoctoral Fellowship at the Santa Fe Institute. S.R. was supported  
 649 by grants DMR-1608211 and 1623243 from the National Science Foundation,  
 650 and by the John Templeton Foundation, all at the Santa Fe Institute.

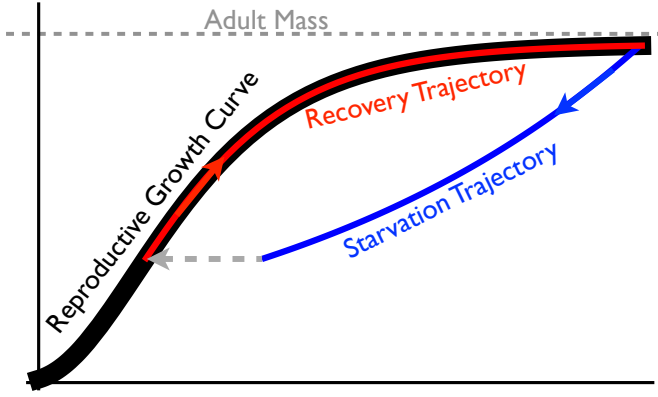


Fig. 1: The growth trajectory over absolute time of an individual organism as a function of body mass. Initial growth follows the red trajectory to an energetically replete adult mass  $M$ . Starvation follows the concave blue trajectory to  $m_{\text{starve}} < M$ , whereas recovery follows the convex growth trajectory from  $m_\sigma$  to  $M$ .

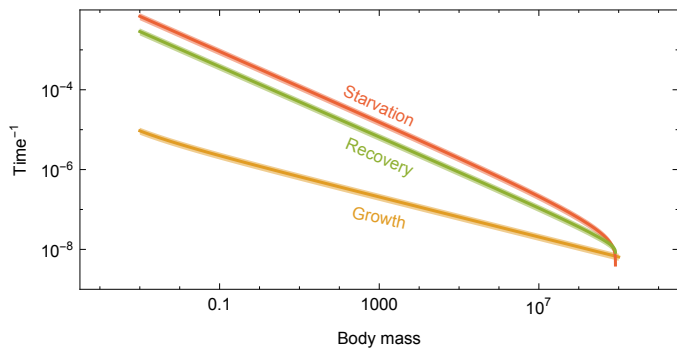


Fig. 2: Allometrically constrained starvation rate  $\sigma$  (red) and recovery rate  $\rho$  relative to the reproductive rate  $\lambda$  (yellow) as a function of body mass. The rate of starvation is greater than the rate of reproduction for all realized terrestrial endotherm body sizes. Mean values  $\pm 20\%$  variation are shown by the shaded region for each rate.

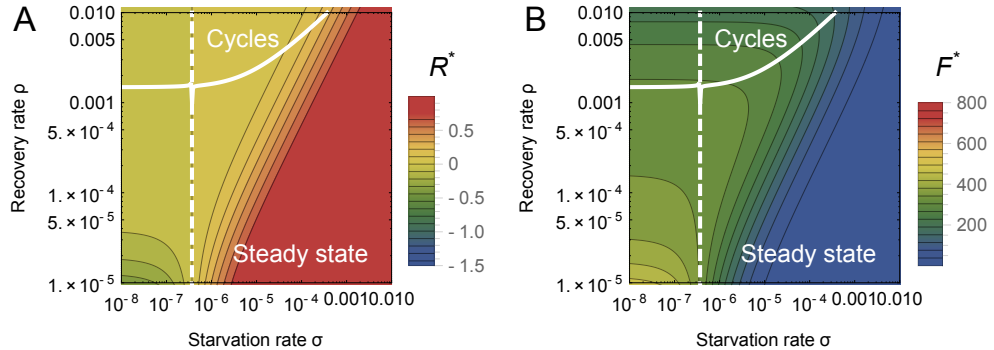


Fig. 3: The transcritical (dashed) and Hopf bifurcation (solid) as a function of the starvation rate  $\sigma$  and recovery rate  $\rho$  for a 100g consumer. These bifurcation conditions separate parameter space into infeasible, cyclic, and steady state dynamic regimes. The color gradient shows the steady state densities for (A) the resource  $R^*$  and the (B) energetically replete consumers  $F^*$ , (warmer colors denote higher densities). Steady state densities for the energetically deficient consumers  $H^*$  (not shown) scale with those for  $F^*$ .

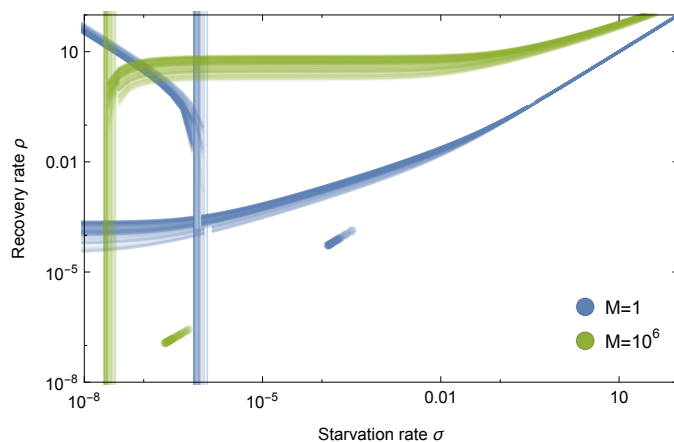


Fig. 4: Transcritical (vertical lines) and Hopf bifurcations (curves) for allometrically determined starvation  $\sigma$  and recovery  $\rho$  rates as a function of different mammalian body sizes:  $M = A \times 10^1\text{g}$  (blue) and  $M = A \times 10^6\text{g}$  (green), where  $A$  is a random uniform variable in [1, 9].

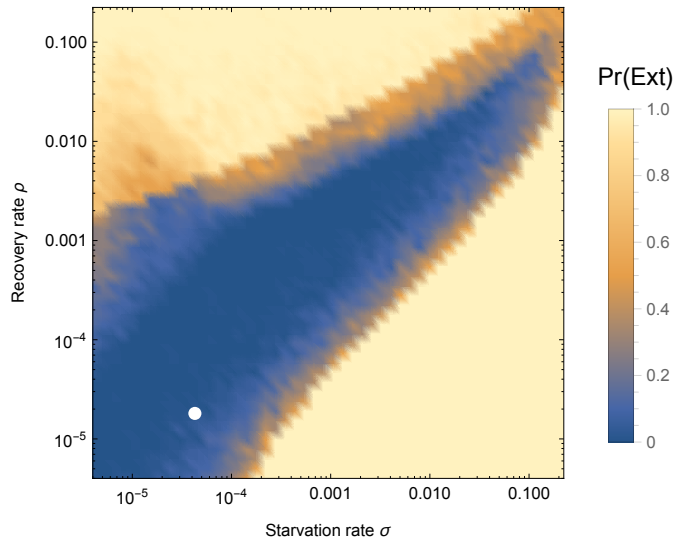


Fig. 5: Probability of extinction for a 100g consumer as a function of the starvation rate  $\sigma$  and recovery rate  $\rho$ , where the initial density is given as  $A(F^*, H^*, R^*)$ , with  $A$  being a random uniform variable in  $[0, 2]$ . Extinction is defined as the population trajectory falling below  $0.1 \times$  the allometrically constrained steady state. The white point denotes the allometrically constrained starvation and recovery rate.

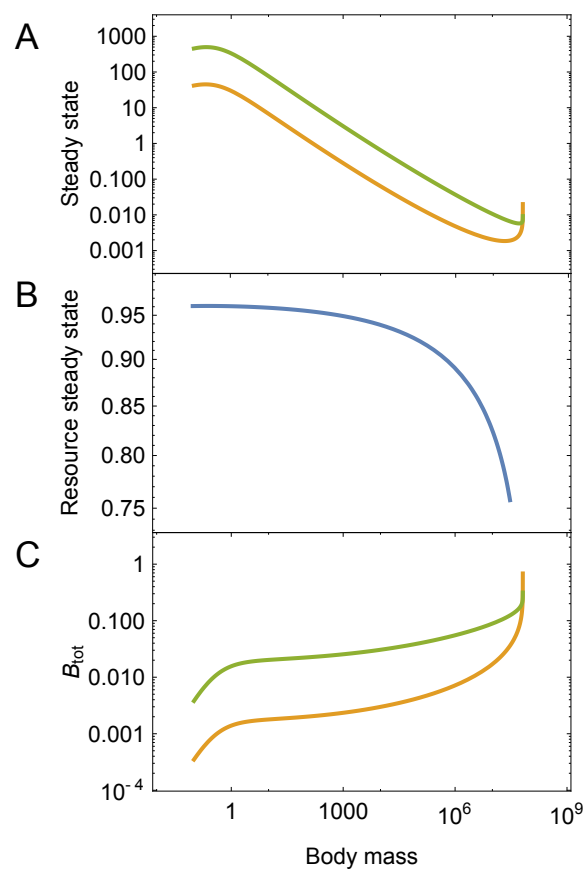


Fig. 6: (A) Consumer steady states  $F^*$  and  $H^*$  as a function of body mass. (B) Resource steady state  $R^*$  as a function of consumer body mass. (C) Total energetic use  $B_{\text{tot}}$  of consumer populations at the steady state as a function of body mass.

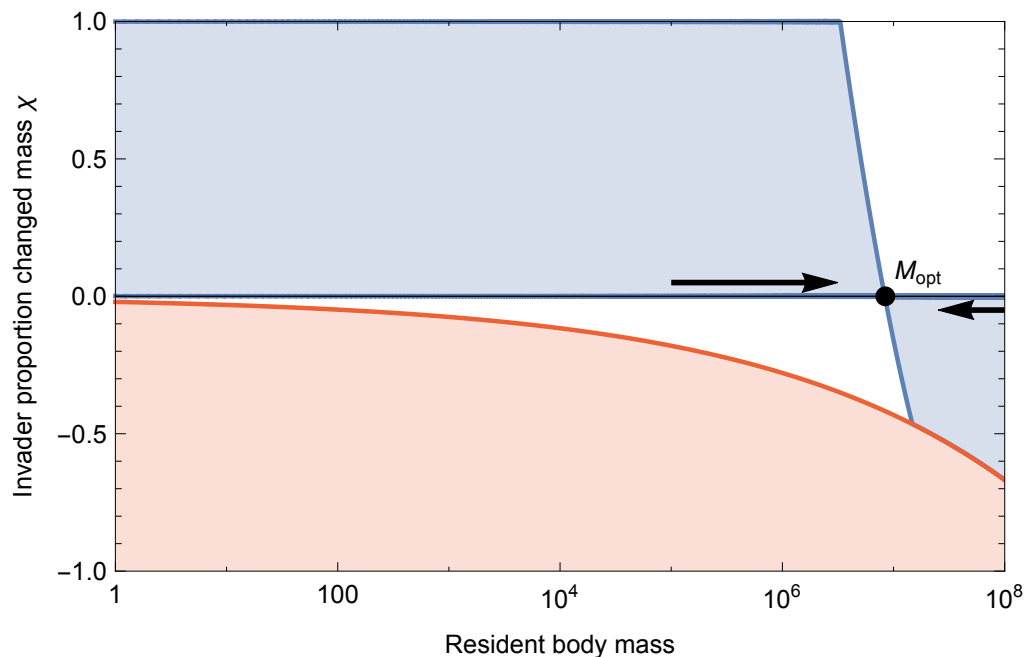


Fig. 7: Invasion feasibility for organisms with a proportional change in mass  $\chi$  against a population with a resident body mass  $M$ . The blue region denotes proportions of modified mass  $\chi$  resulting in successful invasion. The red region denotes values of  $\chi$  that result in a mass that is below the starvation threshold and is thus infeasible. Arrows point to the predicted optimal mass  $M_{\text{opt}} = 8.43 \times 10^6$ , which serves as the evolutionary stable state.